iScience

CellPress
OPEN ACCESS

Article

Dynein and muskelin control myosin VI delivery towards the neuronal nucleus

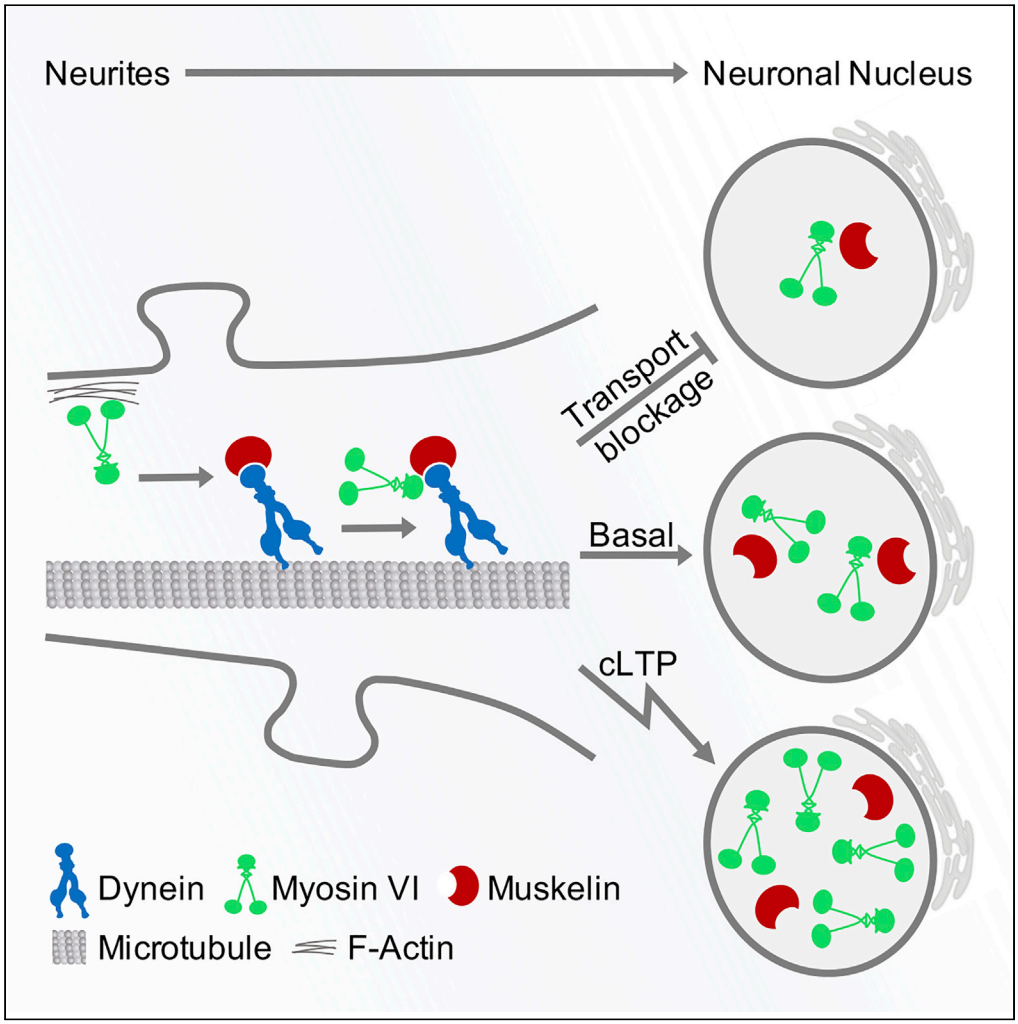

Matthias Kneussel, Noelia Sánchez-Rodríguez, Michaela Mischak, Frank F. Heisler

frank.heisler@zmnh.uni-hamburg.de (F.F.H.)
matthias.kneussel@zmnh.uni-hamburg.de (M.K.)

Highlights

Myosin VI and muskelin are recruited to the neuronal nucleus

Active cytoplasmic dynein is required for myosin VI and muskelin nuclear targeting

Muskelin regulates myosin VI to dynein binding and myosin VI nuclear translocation

Dynein mediates nuclear translocation of myosin VI during cLTP

Kneussel et al., iScience 24, 102416
May 21, 2021
https://doi.org/10.1016/j.isci.2021.102416

iScience

CellPress
OPEN ACCESS

Article

Dynein and muskelin control myosin VI delivery towards the neuronal nucleus

Matthias Kneussel,[1,*] Noelia Sánchez-Rodríguez,[1,2] Michaela Mischak,[1,2] and Frank F. Heisler[1,3,*]

SUMMARY

Protein transport toward the nucleus is important for translating molecular signals into gene expression changes. Interestingly, the unconventional motor protein myosin VI regulates RNA polymerase II-dependent gene transcription. Whether actin-filament-dependent myosins are actively transported to nuclear compartments remains unknown.

Here, we report that neurons also contain myosin VI inside their nucleus. Notably, nuclear appearance of this actin-dependent motor depends on functional cytoplasmic dynein, a minus end-directed microtubule motor. We find that the trafficking factor muskelin assists in the formation of dynein-myosin VI interactions and further localizes to nuclear foci, enriched in the myosin. Impairment of dynein, but not myosin VI function, reduces nuclear muskelin levels. In turn, muskelin represents a critical determinant in regulating myosin VI nuclear targeting.

Our data reveal that minus end-directed microtubule transport determines myosin VI subcellular localization. They suggest a pathway of cytoplasm-to-nucleus trafficking that requires muskelin and is based on dynein-myosin cross talk.

INTRODUCTION

Molecular motors execute a variety of critical processes within various cell types. The families of kinesins and dyneins represent microtubule (MT)-associated ATPases, whereas the myosin family motor proteins perform cellular processes associated with the actin cytoskeleton (Hirokawa et al., 2010; Schliwa and Woehlke, 2003; Vale, 2003). Although kinesins and dynein mainly act within the cytoplasm, recent evidence points to important roles of specific myosins in mammalian nuclei (Cook et al., 2020).

Cytoplasmic dynein is the key MT minus end-directed motor essential for long-distance transport and positioning of organelles, vesicular cargoes, and cytoplasmic molecules (Reck-Peterson et al., 2018). The dynein transport machinery consists of the dynein complex, the dynactin complex required for movement along MTs, and coiled-coil-containing activating proteins. In neurons, due to their highly polarized architecture, dynein often transports cargoes from the cell periphery to the cell body, as observed for the endo-lysosomal trafficking of neurotransmitter receptors (Heisler et al., 2011; Maas et al., 2006) and other synaptic proteins (Boecker and Holzbaur, 2019; Heisler et al., 2018; Schapitz et al., 2010). The specificity of cargo selection and the regulation of motor activities are often achieved through adaptor and accessory transport factors (Heisler et al., 2014; Kneussel et al., 2014; Olenick and Holzbaur, 2019; Reck-Peterson et al., 2018). Although dynein is suggested to functionally associate with kinesin-1 motor complexes for bidirectional cargo trafficking and self-positioning (Olenick and Holzbaur, 2019), the cross talk of molecular motors between the actin and MT cytoskeleton remains largely unexplored (Coles and Bradke, 2015).

Cytoplasmic dynein mainly promotes long-distance transport of cargoes along MT tracks, whereas actin-based myosin VI functions include the regulation of Golgi complex integrity, F-actin dynamics, and cell migration (Kneussel and Wagner, 2013; Tumbarello et al., 2013). Besides myosin VI's ability to act as a load-dependent anchor (Altman et al., 2004), it represents a unique myosin family member that moves to F-actin minus ends (Wells et al., 1999). At the cell cortex and in synaptic spines, myosin VI regulates vesicular trafficking and the endocytosis of neurotransmitter receptors (Buss et al., 2001; Heisler et al., 2011; Morris et al., 2002; Osterweil et al., 2005; Wagner et al., 2019). The cytoplasmic role of myosin VI and its structural properties have been thoroughly investigated (Tumbarello et al., 2013), whereas actin and

[1]Department of Molecular Neurogenetics, Center for Molecular Neurobiology, ZMNH, University Medical Center Hamburg-Eppendorf, Falkenried 94, 20251 Hamburg, Germany

[2]These authors contributed equally

[3]Lead contact

*Correspondence: frank.heisler@zmnh.uni-hamburg.de (F.F.H.), matthias.kneussel@zmnh.uni-hamburg.de (M.K.)

https://doi.org/10.1016/j.isci.2021.102416

myosin VI notably exist in the mammalian nucleus with their nuclear functions only being about to be unraveled (Cook et al., 2020).

Within nuclei, myosin VI was identified to associate with RNA polymerase II (RNAPII) (Vreugde et al., 2006) and to functionally regulate hormone and cytokine receptor-dependent gene transcription (Fili et al., 2017, 2020; Loikkanen et al., 2009; Zorca et al., 2015). Mechanistically, myosin VI was suggested to function as an auxiliary motor for RNAPII to drive gene expression while undergoing regulated and direct DNA binding (Fili et al., 2017, 2020; Vreugde et al., 2006). Only recently, the active movement of myosin VI along actin filaments in the nucleus was also detected (Grosse-Berkenbusch et al., 2020). The functions of myosin VI inside the nucleus include transcription-dependent chromatin rearrangements (Grosse-Berkenbusch et al., 2020), gene pairing (Zorca et al., 2015), and the spatial organization of transcription initiation (Hari-Gupta et al., 2020). A role of the myosin in gene transcription is further supported by studies of the p53-dependent pro-survival pathway (Cho and Chen, 2010; Jung et al., 2006) where it was found to redistribute from cytoplasmic to nuclear compartments upon DNA damage. Interestingly, myosin VI nuclear accumulation was also increased after stimulation of neuroendocrine PC12 cells (Majewski et al., 2018) and after serum stimulation of HeLa cells (Hari-Gupta et al., 2020). These observations suggest that active molecular processes might underlie myosin VI nuclear appearance. Whether myosin VI localizes to neuronal nuclei in mammalian brain as well as the molecular factors that might transport the myosin for its potential active nuclear targeting in general remain unknown.

Muskelin is an evolutionary conserved protein expressed in various tissues. It was originally identified to mediate cell adhesive and actin cytoskeletal responses (Adams et al., 1998) and to act as an integrator of cell morphology and nucleocytoplasmic communication in skeletal myoblasts (Valiyaveettil et al., 2008). Of note, in muscle cells myosin VI localization to nuclei was also observed (Karolczak et al., 2013). Recent studies described muskelin as a functional component of the CTLH complex, a macromolecular assembly suggested to reside either in the cytoplasm or in the nucleus and to integrate fundamental processes including energy metabolism, proliferation, survival, cell adhesion, and migration in response to extracellular stimuli (Huffman et al., 2019; Lampert et al., 2018; Liu and Pfirrmann, 2019; Maitland et al., 2019; Qiao et al., 2020).

In neurons, muskelin critically regulates the bidirectional vesicular transport of $GABA_A$ receptors and of the cellular prion protein PrP^C (Heisler et al., 2011, 2018). It acts as a cargo adaptor, directly linking synaptic proteins to cytoplasmic dynein and has been suggested to regulate the activity of vesicular motor protein assemblies (Heisler et al., 2011, 2018). Interestingly, muskelin represents one of the few transport factors that associates with both MT-based motor proteins and the actin-dependent motor myosin VI to regulate $GABA_A$ receptor endocytosis (Heisler et al., 2011, 2018). Whether muskelin or the MT motor dynein affect transport and positioning of actin-dependent myosin motor proteins is presently unknown.

In this study we show that the actin-dependent motor protein myosin VI localizes to neuronal nuclei, depending on active transport through the MT-dependent dynein motor complex. Myosin VI nuclear targeting critically requires muskelin, a trafficking regulator known to associate with both motor systems. Our data suggest a cellular pathway that is based on myosin-dynein cross talk.

RESULTS

Myosin VI associates with dynein and is transported to the neuronal nucleus

Myosin VI was found in the nucleus of various cell types and is suggested to functionally regulate nuclear processes (Karolczak et al., 2013; Majewski et al., 2018; Vreugde et al., 2006; Zorca et al., 2015). In neurons, the myosin motor mediates critical functions at the cellular cortex in regulating synaptic transport and plasticity (Heisler et al., 2011; Wagner et al., 2019), but whether and how myosin VI undergoes nuclear translocation in neuronal cell types has remained unknown.

We therefore isolated nuclear proteins from mouse whole brain tissue. Detection of the NMDA receptor subunit GluN2B and the neuron-specific nuclear protein NeuN (Mullen et al., 1992) served as quality controls, as they are restricted to the cytoplasmic (C) or nuclear extract (N), respectively (Figure 1A). Besides the presence of myosin VI in the cytoplasm, we detected prominent proportions in the nuclei of brain cells (Figure 1A). Likewise, actin was present in both, cytoplasmic and nuclear fractions. To verify the specificity of the myosin VI antibody used in this experiment, we prepared nuclear extracts derived from brains of

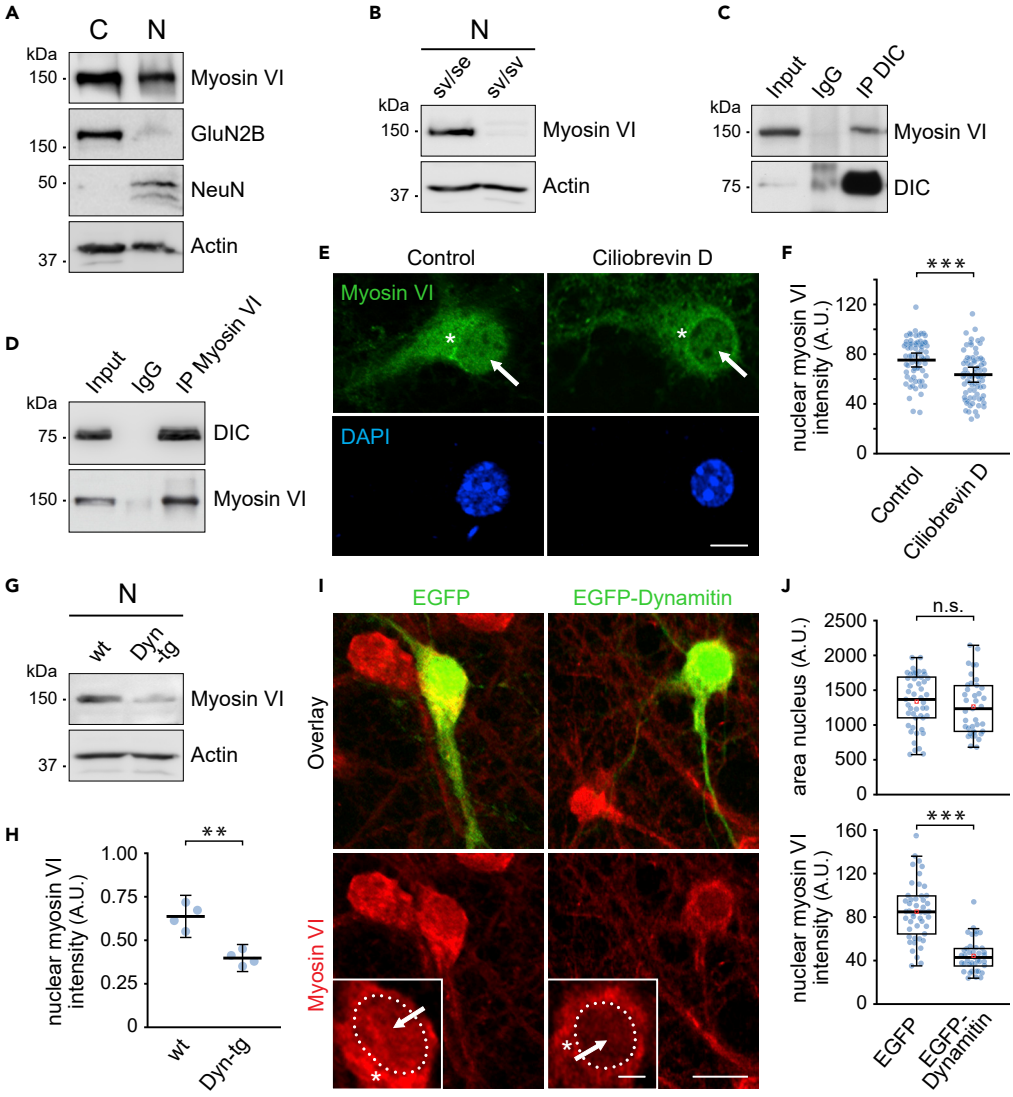

Figure 1. Myosin VI nuclear targeting depends on dynein

(A) Myosin VI is detected in cytoplasmic (C) and nuclear fractions (N) from adult mouse brain (n = 3 experiments).

(B) Anti-myosin VI antibody specificity control in nuclear fractions (N) from homozygous (sv/sv) and heterozygous (sv/se) Snell's waltzer mice. Control: Actin.

(C) Immunoprecipitation using DIC-specific antibodies coprecipitates myosin VI from whole brain lysate in the presence of 1% Triton X-100 (n = 3 experiments).

(D) Coimmunoprecipitation of DIC with myosin VI from whole brain lysate in the presence of 1% Triton X-100 (n = 3 experiments).

(E) Confocal images showing myosin VI nuclear intensity (arrows) after immunostaining of days in vitro (DIV) 12–14 hippocampal neurons treated for 80 min with 0.4% DMSO (control) or 20 μM ciliobrevin D. Scale bar, 10 μm.

(F) Reduced nuclear myosin VI intensity in ciliobrevin D (62.25 ± 4.15) when compared with control (75.74 ± 3.98) treated neurons. Control: n = 69 cells; ciliobrevin D: n = 77 cells; 3 experiments. Data represent mean ± the 95% confidence intervals for the mean. Independent samples t test, $p < 0.001$, *** indicates statistical significance.

(G) Nuclear fractions (N) from brain of dynamitin-overexpressing (Dyn-tg) and wild-type (wt) mice.

(H) Reduced nuclear myosin VI levels in Dyn-tg (0.40 ± 0.07) when compared with wt mice (0.64 ± 0.12) (n = 4 experiments). Myosin VI intensities normalized to Actin. Data represent mean ± the 95% confidence intervals for the mean. Independent samples t test, $p < 0.01$, ** indicates statistical significance.

(I) Confocal images showing myosin VI nuclear intensity (arrows) after immunostaining of DIV 12–14 hippocampal neurons overexpressing EGFP or EGFP-dynamitin. Scale bar: 20 μm and 5 μm in insets.

(J) No significant differences in nuclear area between EGFP-dynamitin- (median = 1,225.00) and EGFP- (median = 1,358.00) overexpressing neurons, Mann-Whitney U test, U = 784.000, Z = −1.149, $p = 0.250$. Reduced nuclear myosin VI

Figure 1. *Continued*
intensity in EGFP-dynamitin- (median = 43.15) when compared with EGFP- (median = 84.82) overexpressing neurons. Distributions differed between groups, two-sample Kolmogorov-Smirnov, $p < 0.001$, and nuclear myosin VI intensity significantly differed between groups, Mann-Whitney U test, $U = 162.00$, $Z = -6.545$, $p < 0.001$, *** indicates statistical significance. EGFP: n = 47 cells; EGFP-dynamitin: n = 39 cells; 4 experiments. Box borders represent the 25th and 75th percentiles, horizontal lines inside boxes indicate median, and whiskers represent values less than 1.5 times the interquartile range lower or higher than the 25th and 75th percentiles, respectively. Red squares indicate the mean.

homozygous (sv/sv) Snell's waltzer mice, representing spontaneous myosin VI null mutants (Avraham et al., 1995). Myosin VI was detectable in the nuclear brain extract from heterozygous animals (sv/se), whereas the myosin VI signal was lost in myosin VI-depleted fractions (sv/sv), when compared with actin, used as control (Figure 1B). We therefore conclude that brain myosin VI generally undergoes translocation to the nuclear compartment.

Whether mammalian myosin VI motors reach the nucleus via passive diffusion or active transport is presently unknown. To gain mechanistic insights into the process of its nuclear accumulation, we asked whether the myosin might bind to other motor proteins, known to mediate active transport toward neuronal somata. Notably, precipitation of endogenous dynein intermediate chain (DIC) from brain lysate resulted in coprecipitation of endogenous myosin VI (Figure 1C), indicating that the myosin motor is found in a protein complex containing the dynein motor. Accordingly, precipitation of myosin VI, vice versa, led to coprecipitation of DIC (Figure 1D). As the experiments were performed in the presence of detergent, we exclude that both motors just share the same transport vesicle. To test whether dynein affects myosin VI subcellular localization, we first treated cultured hippocampal neurons with ciliobrevin D (Cilio D), a specific inhibitor of the AAA+ ATPase activity of the dynein motor domain (Firestone et al., 2012). Under control conditions, immunostaining revealed high myosin VI signals in the somatic regions close to the neuronal nucleus (Figures 1E and 1I, asterisks), which likely represent the role of myosin VI in Golgi organization (Jung et al., 2006; Sahlender et al., 2005; Tumbarello et al., 2013). In addition, neuronal myosin VI was detectable as punctate signals inside the nuclei (Figures 1E and 1I, arrows). However, the acute treatment of hippocampal neurons with Cilio D caused a moderate but significant reduction in myosin VI nuclear signal intensity (Figures 1E and 1F). These data suggest that the nuclear delivery of myosin VI requires active dynein-based cytoskeleton transport.

To validate this finding, we next applied an independent loss-of-function approach using transgenic mice that overexpress dynamitin in the brain (LaMonte et al., 2002; Perlson et al., 2009). Dynamitin is a subunit of the dynactin complex associated with dynein, and its overexpression leads to dynein-dynactin dissociation (Burkhardt et al., 1997; King and Schroer, 2000; Palazzo et al., 2001; Valetti et al., 1999). Overexpressed dynamitin has been shown to effectively interfere with dynactin- and dynein-mediated processes such as Golgi dynamics and cargo transport, including neuronal trafficking. Notably, the levels of myosin VI but not of actin (control) were significantly decreased in nuclear fractions derived from dynamitin-overexpressing mice (Dyn-tg), when compared with wild-type fractions (Figures 1G and 1H). We next aimed to test whether these results would similarly apply to hippocampal neurons. To interfere with dynein-mediated transport, we therefore overexpressed EGFP-dynamitin (Burkhardt et al., 1997). Although this condition did not alter the average area of neuronal nuclei, it strongly reduced myosin VI signal intensity within the nuclear compartment (Figures 1I and 1J).

Together, our data suggest that the MT-dependent motor dynein piggybacks the myosin VI motor to promote its nuclear translocation.

The microtubule- and actin-associated transport factor muskelin enters neuronal nuclei

The transport factor muskelin is one of the few cargo adaptors that associates with both actin-dependent myosin VI and MT-based dynein motor complexes, to interconnect subsequent steps of cytoplasmic cargo trafficking (Heisler et al., 2011, 2018). Interestingly, fluorescent fusion proteins of muskelin mutants were reported to differentially enter the nucleus in skeletal myoblasts and neurons (Delto et al., 2015; Valiyaveettil et al., 2008).

To assess whether muskelin could be involved in dynein-mediated nuclear targeting of myosin VI, we initially performed cellular fractionation experiments to further characterize the subcellular localization of endogenous muskelin in murine brain. Following isolation of proteins from whole brain tissue, we

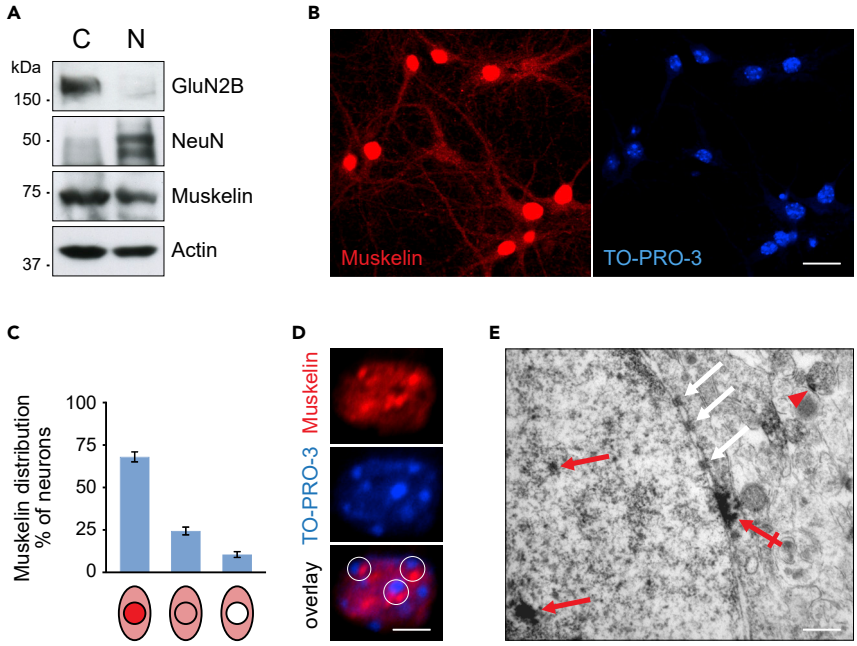

Figure 2. Localization of muskelin in neuronal nuclei

(A) Cytoplasmic (C) and nuclear extracts (N) after cell fractionation from adult mouse brain contain muskelin (n = 3 experiments).

(B) Immunostainings of muskelin in DIV 12–14 hippocampal neurons with TO-PRO-3 colabeling reveals strong nuclear muskelin signals. Scale bar, 20 μm.

(C) Quantification of (B) indicating that 67.17% ± 0.03% of neurons show muskelin nuclear enrichment, 25.35% ± 0.02% cells show equal muskelin intensities across soma and nuclei, and 7.48% ± 0.01% show less muskelin in nuclear when compared to somatic regions (331 neurons, n = 3 experiments). Data represent mean ± SEM.

(D) Immunostaining of muskelin with TO-PRO-3 labeling in DIV 12–14 hippocampal neurons show punctate muskelin signals adjacent to TO-PRO-3 foci (circles) within the nucleus (n = 3 experiments). Scale bar, 5 μm.

(E) Electron microscopy showing muskelin-specific immunoperoxidase signals in hippocampal tissue slices from adult mice. Muskelin signals are detected at vesicular structures outside the nucleus (red arrowhead), at the nuclear envelope (crossed red arrow) and within the nucleus (red arrows). White arrows indicate nuclear pores. Scale bar, 50 nm.

identified muskelin in both cytoplasmic (C) and nuclear (N) extracts (Figure 2A). In contrast, the NMDA receptor subunit GluN2B and the neuron-specific nuclear protein NeuN, used as fractionation controls, were restricted to the cytoplasmic or nuclear extract, respectively (Figure 2A). Upon immunostaining of endogenous protein in cultured hippocampal neurons, we further confirmed the nuclear localization of muskelin (Figure 2B). Quantification revealed that about 67% of all cells showed an enrichment of the transport factor within their nuclei, whereas only 7% of the cells turned out negative for nuclear muskelin under neuron culture conditions (Figure 2C). Within the neuronal nucleus, muskelin displayed a punctate distribution. Areas of highest muskelin intensities were frequently detected adjacent to foci of TO-PRO-3-labeled DNA (Figure 2D), representing potential regions of high chromatin density (Falk et al., 2008). We further performed electron microscopy (EM) to analyze cytoplasmic and nuclear muskelin at higher resolution. Consistent with its role as a transport regulator (Heisler et al., 2011, 2018), immunodetection at the ultrastructural level confirmed muskelin at vesicular structures in the cytoplasm (Figure 2E, red arrowhead). In addition, EM revealed distinct muskelin-positive aggregates within the neuronal nucleus (Figure 2E, red arrows) and at the nuclear envelope (Figure 2E, red crossed arrow) of mouse hippocampal slices. Together, these results suggest a potential contribution of muskelin to nuclear functions in neurons.

Cytoplasmic dynein regulates nuclear muskelin levels

The neuron-specific dynein intermediate chain isoform 1a (DIC1a) directly links muskelin to the dynein motor complex (Heisler et al., 2011). In addition to muskelin's role as a coordinator of dynein-mediated transport (Heisler et al., 2011, 2018), we asked whether muskelin itself might require active dynein for its own nuclear delivery.

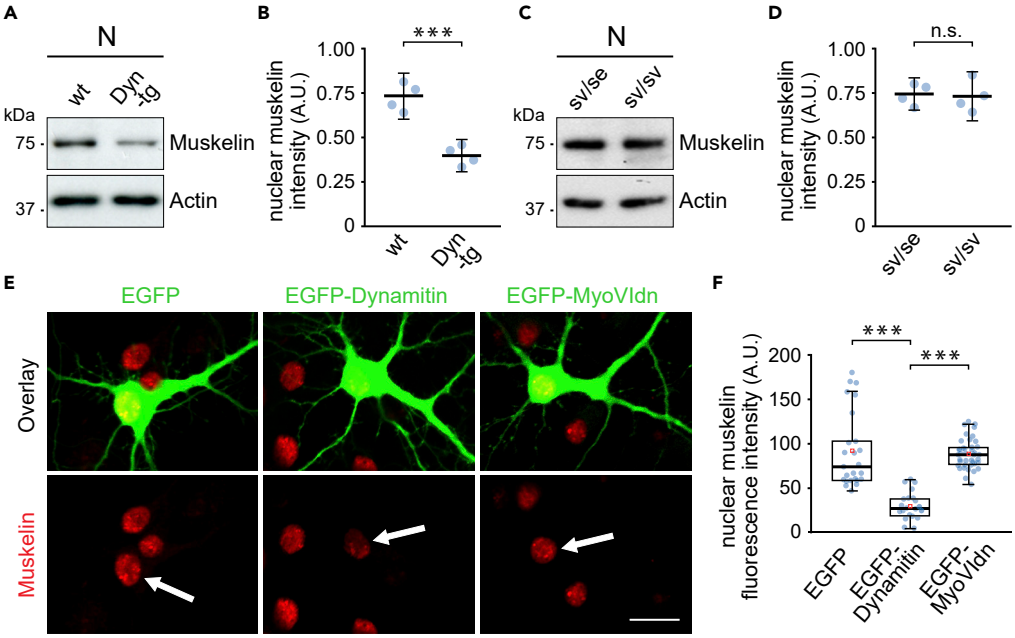

Figure 3. Dynein drives muskelin nuclear targeting

(A) Nuclear fractions (N) from brain of dynamitin-overexpressing (Dyn-tg) and wild-type (wt) mice.

(B) Reduced nuclear muskelin levels in Dyn-tg (0.41 ± 0.09) when compared with wt mice (0.73 ± 0.13) (n = 4 experiments). Muskelin intensities normalized to Actin. Data represent mean ± the 95% confidence intervals for the mean. Independent samples t test, $p < 0.001$, *** indicates statistical significance.

(C) Nuclear fractions (N) from brain of homozygous (sv/sv) and heterozygous (sv/se) Snell's waltzer mice.

(D) No significant differences in muskelin nuclear levels in sv/sv (0.73 ± 0.14) when compared with sv/se mice (0.74 ± 0.09) (n = 4 experiments). Muskelin intensities normalized to Actin. Data represent mean ± 95% confidence intervals for the mean. Independent samples t test, $p = 0.833$, n.s.: not statistically significant.

(E) Confocal images of nuclear muskelin intensity (arrows) upon immunostaining of DIV 12–14 hippocampal neurons overexpressing EGFP, EGFP-dynamitin, or EGFP-MyoVIdn as indicated. Scale bar, 20 μm.

(F) Nuclear muskelin fluorescence intensity was significantly different between at least one pair of groups, Kruskal-Wallis test, χ^2 (2) = 45.869, $p < 0.001$. Dunn's pairwise multiple comparisons test (p values adjusted using Bonferroni correction) revealed significant differences between EGFP-dynamitin (median = 24.36) and EGFP (median = 72.21), $z = 5.113$, $p < 0.001$, and between EGFP-dynamitin and EGFP-MyoVIdn (median = 85.78), $z = -6.616$, $p < 0.001$. *** indicates statistical significance. There was no evidence of difference between EGFP and EGFP-MyoVIdn, $p = 0.872$. EGFP: n = 25 cells; EGFP-dynamitin: n = 21 cells; EGFP-MyoVIdn: n = 40 cells; 3 experiments. Box borders indicate the 25th and 75th percentiles, horizontal lines inside boxes indicate median, and whiskers represent values less than 1.5 times the interquartile range lower or higher than the 25th and 75th percentiles, respectively. Red squares indicate the mean.

Using dynamitin-overexpressing transgenic mice, impaired in neuronal dynein-mediated transport (La-Monte et al., 2002; Perlson et al., 2009), we found that muskelin levels were significantly reduced in nuclear fractions of transgenes (Dyn-tg), when compared with wild-type and loading controls (Figures 3A and 3B). These data indicate that muskelin is actively translocated to the neuronal nucleus and that this process depends on functional dynein.

Based on the fact that muskelin also associates with the actin-dependent motor myosin VI (Heisler et al., 2011), we further aimed to investigate whether the myosin may potentially contribute to regulate nuclear muskelin levels. However, in contrast to the functional inhibition of the MT-dependent motor dynein, depletion of the actin-dependent motor myosin VI in homozygous Snell's waltzer mice (sv/sv) (Avraham et al., 1995) did not affect muskelin levels in nuclear brain fractions (Figures 3C and 3D). In an independent assay, we overexpressed EGFP-dynamitin (Burkhardt et al., 1997) or a dominant-negative myosin VI mutant EGFP-MyoVIdn (Heisler et al., 2011; Osterweil et al., 2005), to test whether these observations would also apply to hippocampal neurons. The fluorescence intensity of nuclear muskelin remained unaffected through EGFP-MyoVIdn, whereas it appeared strongly reduced in neurons overexpressing EGFP-

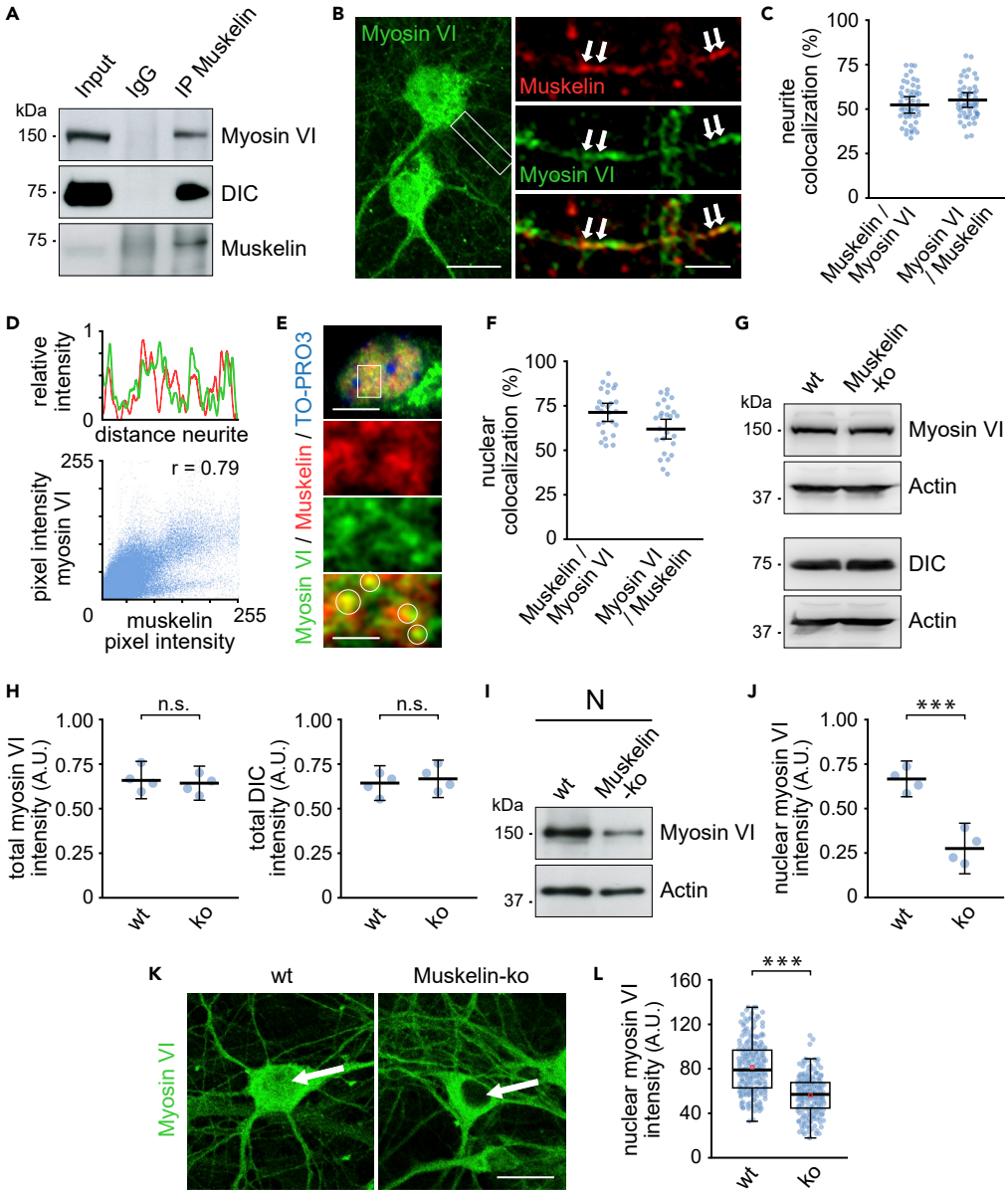

Figure 4. Muskelin regulates myosin VI nuclear targeting

(A) Myosin VI and dynein coprecipitate with muskelin after immunoprecipitation from whole brain lysate in the presence of 1% Triton X-100 (n = 3 experiments).

(B) Coimmunostaining of myosin VI and muskelin in DIV 12–14 hippocampal neurons. Arrows in magnified region (boxed region) indicate myosin VI and muskelin colocalization in dendrites. Scale bars: 20 μm in overview, 5 μm in boxes.

(C) Quantification: % of muskelin signals overlapping myosin VI (52.22 ± 3.06), % of myosin VI signals overlapping muskelin (54.94 ± 2.75), n = 52 cells; 4 experiments. Data represent mean ± 95% confidence intervals for the mean.

(D) Upper plot: Line scan of (B) showing muskelin (red) and myosin VI (green) intensities along the dendrite segment. Lower plot: Scatterplot showing correlation (Pearson correlation coefficient r = 0.79) between myosin VI and muskelin pixel intensities.

(E) Coimmunostaining detects muskelin and myosin VI colocalized puncta (circles) in nuclei (TO-PRO-3 labeling) of DIV 12–14 hippocampal neurons. Boxed nuclear region is shown at higher magnification. Scale bars: 10 μm in overview, 3 μm in boxes.

(F) Quantification: % of muskelin signals overlapping myosin VI (70.91 ± 4.73), % of myosin VI signals overlapping muskelin (62.49 ± 5.61), n = 26 cells; 4 experiments. Data represent mean ± 95% confidence intervals for the mean.

(G) Whole brain lysate of muskelin knockout (Muskelin-ko) and wild-type (wt) mice.

Figure 4. *Continued*

(H) No statistically significant differences in total myosin VI or DIC levels between wt (Myo VI: 0.67 ± 0.11; DIC: 0.64 ± 0.10) and ko brain lysate (Myo VI: 0.64 ± 0.08; DIC: 0.68 ± 0.11) (n = 4 experiments). Myosin VI intensities normalized to Actin. Data represent mean ± the 95% confidence intervals for the mean. Independent samples t test, p = 0.441 (Myo VI); p = 0.433 (DIC), n.s.: not statistically significant.

(I) Nuclear extracts (N) from adult brains of muskelin knockout and wild-type mice.

(J) Reduced nuclear myosin VI levels in Muskelin-ko (0.28 ± 0.15) compared with wt mice (0.66 ± 0.10) (n = 4 experiments). Myosin VI intensities normalized to Actin. Data represent mean ± 95% confidence intervals for the mean. Independent samples t test, $p < 0.001$, *** indicates statistical significance.

(K) Confocal images of nuclear myosin VI intensity (arrows) upon immunostaining of DIV 12–14 hippocampal neurons from muskelin knockout or wild-type mice. Scale bar, 20 μm.

(L) Reduced nuclear myosin VI intensity in Muskelin-ko (median = 56.41) when compared with wt (median = 78.21) neurons. Distributions differed between both groups, two-sample Kolmogorov-Smirnov, $p < 0.001$, and nuclear myosin VI intensity significantly differed between both groups, Mann-Whitney U test, U = 10,324.00, Z = −11.115, $p < 0.001$, *** indicates statistical significance. Muskelin-ko: n = 219 cells; wt: n = 237 cells; 4 experiments. Box borders represent the 25th and 75th percentiles, horizontal lines inside boxes indicate median, and whiskers represent values less than 1.5 times the interquartile range lower or higher than the 25th and 75th percentiles, respectively. Red squares indicate the mean.

dynamitin (Figures 3E and 3F). Our findings therefore indicate that dynein, but not myosin VI, is the critical driver to power muskelin translocation toward the neuronal nucleus.

Muskelin regulates myosin VI nuclear targeting

A former study on neurotransmitter receptor endocytosis had revealed subsequent steps of muskelin association with either myosin VI or dynein motor complexes (Heisler et al., 2011). In addition, we find that myosin VI motor can in general interact with cytoplasmic dynein (compare with Figures 1C and 1D). We therefore aimed to understand whether muskelin may be part of a triple myosin VI-dynein complex and whether it would act on myosin VI nuclear delivery.

Indeed, coimmunoprecipitation experiments detected dynein and myosin VI to coprecipitate with muskelin (Figure 4A), suggesting that muskelin associates with both molecular motors at a given time. As these experiments were performed in the presence of detergent, we exclude that the proteins just share identical vesicles. Furthermore, we observed a strong correlation and frequent colocalization of muskelin and myosin VI signals in proximal dendrites of hippocampal neurons following coimmunostaining (Figures 4B–4D). Based on muskelin's role in neuronal trafficking, the colocalized signals potentially represent molecules in transit. In addition to colocalization in dendrites, we detected a frequent overlap of muskelin and myosin VI puncta in the neuronal nucleus (Figures 4E and 4F). To test whether muskelin controls myosin VI nuclear targeting, we then analyzed brain fractions from muskelin knockout mice (Muskelin-ko) (Heisler et al., 2011). The overall levels of myosin VI and dynein in total brain fractions equaled between genotypes, indicating that muskelin does not affect the expression or degradation of the motor proteins (Figures 4G and 4H). However, nuclear protein levels of myosin VI were strongly reduced in muskelin-deficient mice, when compared with wild-type and loading controls (Figures 4I and 4J). These results were also confirmed in a second and neuron-specific approach. Following immunostaining of cultured hippocampal neurons, we found that muskelin deficiency (Muskelin-ko) caused a significant decrease in myosin VI signals in the neuronal nucleus (Figures 4K and 4L).

With respect to a functional triple complex harboring muskelin and the two motor proteins (compare with Figure 4A), we hypothesized that reduced nuclear myosin VI levels in muskelin-depleted neurons might be due to impaired myosin VI to dynein binding in the absence of muskelin. Notably, coprecipitation of DIC with myosin VI was significantly reduced in muskelin-depleted brain lysate (Muskelin-ko), compared with lysate obtained from wild-type mice (wt) (Figures 5A and 5B). This suggests that muskelin assists in the formation of a dynein-myosin VI interaction. As myosin VI has been shown to undergo stimuli-dependent nuclear translocation in several cell lines (Cho and Chen, 2010; Hari-Gupta et al., 2020; Jung et al., 2006; Majewski et al., 2018), we finally asked whether the localization of neuronal myosin VI would respond to neuron-specific stimulation paradigms. Indeed, immunostainings of hippocampal neurons revealed a significant increase of nuclear myosin VI intensity, following 30 min of recovery after induction of chemical long-term potentiation (cLTP) (Figures 5C–5E) (Franchini et al., 2019; Otmakhov et al., 2004). Furthermore, whereas nuclear myosin VI levels were reduced in neurons treated with Cilio D, induction of cLTP in the presence of Cilio D (Cilio D + cLTP) did not cause an increase in nuclear myosin VI levels that was observed

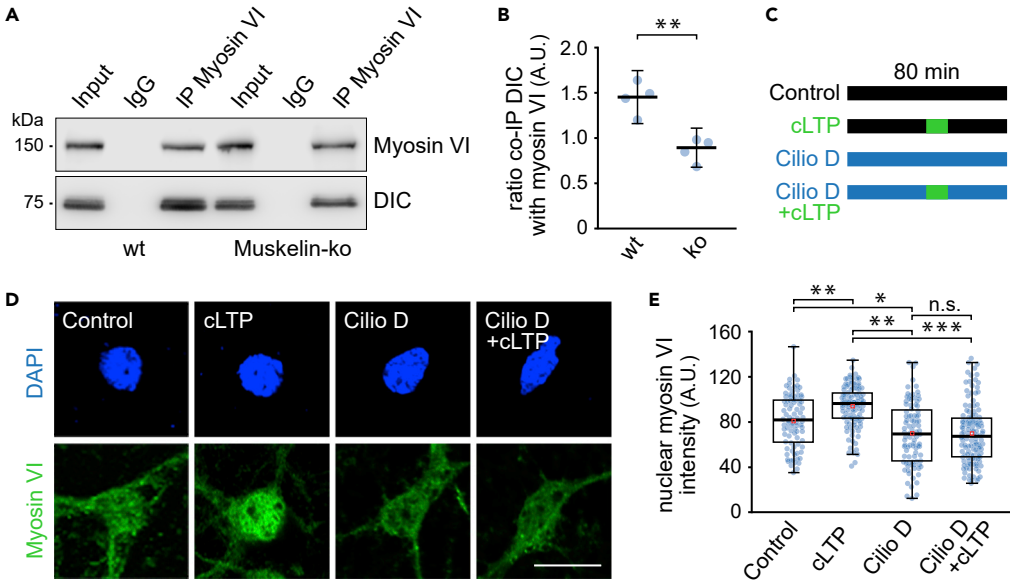

Figure 5. cLTP-induced nuclear translocation of myosin VI

(A) Coprecipitation of DIC with myosin VI after immunoprecipitation in the presence of 1% Triton X-100 using brain lysate from wild-type or muskelin knockout mice.

(B) Reduced coprecipitation of DIC with myosin VI using Muskelin-ko (0.87 ± 0.21) when compared with wt lysate (1.44 ± 0.29). DIC coprecipitation was normalized to myosin VI immunoprecipitation (n = 4 experiments). Data represent mean ± 95% confidence intervals for the mean. Independent samples t test, $p < 0.01$, ** indicates statistical significance.

(C and D) (C) cLTP and ciliobrevin treatment scheme (D) Confocal images showing nuclear myosin VI intensity upon immunostaining of DIV 12–14 hippocampal neurons treated with 0.4% DMSO (control) or 20 μM ciliobrevin D (cilio D) for 80 min or with additional cLTP induction after 40 min during control (cLTP) or ciliobrevin D treatment (cilio D + cLTP). Scale bar, 20 μm.

(E) Nuclear myosin VI intensity was significantly different between at least one pair of groups, Kruskal-Wallis test, χ^2 (2) = 72.561, $p < 0.001$. Dunn's pairwise multiple comparisons test (p values adjusted using Bonferroni correction) revealed significant differences between control (median = 80.95) and cLTP (median = 95.85), $z = -3.572$, $p < 0.01$, ** indicates statistical significance; between cilio D (median = 68.77) and control, $z = 2.821$, $p < 0.05$, * indicates statistical significance; between cilio D and cLTP, $z = -6.678$, $p < 0.01$, ** indicates statistical significance; and between cilio D + cLTP (median = 66.46) and cLTP, $z = 7.775$, $p < 0.001$, *** indicates statistical significance. There was no evidence of difference between cilio D + cLTP and cilio D. Control: n = 86 cells; cilio D: n = 93 cells; cLTP: n = 115 cells; cilio D + cLTP: n = 130 cells; 3 experiments. Box borders indicate the 25th and 75th percentiles, horizontal lines inside boxes indicate median, and whiskers represent values less than 1.5 times the interquartile range lower or higher than the 25th and 75th percentiles, respectively. Red squares indicate the mean.

for neurons treated with cLTP alone (Figures 5C–5E). These data indicate that dynein-dependent processes contribute to the nuclear translocation of myosin VI following cLTP stimulation.

In summary, our findings identify myosin VI in neuronal nuclei and suggest a mechanism, by which dynein piggybacks myosin VI to regulate its nuclear trafficking. Using transgenic, mutant, and KO mice, we characterized muskelin's and myosin VI's nuclear entry and suggest muskelin to regulate the active transport of myosin VI toward the nuclear compartment.

DISCUSSION

In this study, we report the association of actin-dependent myosin VI with the MT-based motor protein dynein. Myosin VI shows a punctate localization in the nucleus of hippocampal neurons and transgenic mice impaired in dynein motor function, or acute inhibition of the dynein ATPase reveals a reduced nuclear targeting of myosin VI. The trafficking factor muskelin assists in the formation of a dynein-myosin VI interaction and also displays a punctate nuclear distribution in the majority of neurons. In contrast, the genetic knockout of muskelin interferes with myosin VI nuclear targeting. Together our findings indicate that myosin VI undergoes active transport toward the nuclear compartment mediated by cytoplasmic dynein in a muskelin-dependent manner.

The presented data connect to previous findings of elevated nuclear myosin VI levels after stimulation of mammalian cell lines (Hari-Gupta et al., 2020; Jung et al., 2006; Majewski et al., 2018). They extend these observations by showing that at least a prominent portion of myosin VI depends on an active transfer toward the mammalian nucleus. Furthermore, the association of the myosin with cytoplasmic dynein and its cargo adaptor muskelin might enable a coordinated nuclear targeting of myosin VI under certain cellular conditions. In this respect, our data identify that neuron-specific stimuli, such as the induction of cLTP, can trigger myosin VI recruitment to the neuronal nucleus. They also provide a first hint that the dynein-muskelin-assisted transport pathway contributes to stimuli-induced myosin VI nuclear translocation.

Although the latter hypothesis requires further investigation, it is supported by the role of dynein in cytoplasm-to-nucleus communication in neuronal tissue. Neurotrophins and their receptors, such as TrkB-BDNF signaling endosomes, undergo nerve terminal-to-soma-directed transport through dynein underlying their downstream nuclear signaling (Gauthier et al., 2004; Heerssen et al., 2004; Olenick et al., 2019). Dynein also associates with cytoplasmic importins and kinases after nerve injury and mediates subsequent retrograde transport to enable nuclear injury responses (Hanz et al., 2003; Perlson et al., 2005). With respect to synaptic signal-to-nucleus communication, dynein binding to the soluble messenger proteins Jacob or CRTC1 was shown to constitute a prerequisite in transmission of stimulus-dependent information from synaptic-to-nuclear compartments (Herbst and Martin, 2017; Karpova et al., 2013; Lever et al., 2015). Together, it is well possible that in addition to cLTP induction, other stimuli might trigger myosin VI nuclear translocation in neurons. Based on myosin VI observations from cell lines, these stimuli might include axonal injury, DNA damage, and pathways of hormone or nutrient signaling in neurons.

In general, it is reasonable to speculate that myosin VI nuclear targeting will underlie a two-step process, by which active dynein first mediates transport toward the nuclear compartment, followed by the shuttling of the myosin across the nuclear envelope. Our data, together with our previous findings (Heisler et al., 2011), suggest that muskelin, as a direct dynein adaptor and myosin VI binding partner at the cell cortex, already coordinates the long-distance delivery of myosin VI toward neuronal somata. In this respect, muskelin might facilitate the association of myosin VI with dynein intermediate chain through direct interaction with DIC involving its LisH/CTLH domain (Heisler et al., 2011, 2018).

However, adding a second level of complexity, proteins harboring these kinds of motifs were in addition reported to substantially provide nuclear localization activity (Emes and Ponting, 2001; Lampert et al., 2018; Qiao et al., 2020; Valiyaveettil et al., 2008). Consistent with this view, the disruption of muskelin dimerization through mutations of its LisH/CTLH domain, thereby exposing this element, triggered the translocation of mRFP-muskelin fusion proteins into the nucleus (Delto et al., 2015). Furthermore, Valiyaveettil et al. also observed nuclear localization activity of muskelin's LisH/CTLH motif by studying GFP fusion proteins and showed that other proteins lacking nuclear import activity were shuttled into mammalian nuclei, when fused to muskelin's LisH/CTLH motif. In summary, (1) the dynein-dependent delivery of myosin VI toward the nucleus and (2) the nuclear import of myosin VI likely represent two distinct highly regulated processes. In parts, these sequential steps might overlap and share some of its multifunctional molecules such as, for instance, muskelin.

In this context it is noteworthy that myosin VI itself also harbors several nuclear localization sequence motifs that seem to be functional (Majewski et al., 2018). A fraction of myosin VI, which already localizes close to the nucleus, might therefore also undergo nuclear entry independent of muskelin. In general, it is plausible that not only one mechanism of nuclear import exists for the myosin (Cook et al., 2020), but also that it undergoes nuclear entry via different pathways. Beside the possibility of an nuclear localization sequence and eventually importin-assisted shuttling across the nuclear envelope, myosin VI nuclear import is likely to be controlled through interactions with other proteins (Cook et al., 2020; Fili et al., 2017; Majewski et al., 2018). Based on our data, we suggest that the dynein-muskelin-assisted pathway is dedicated to coordinate the long-distance delivery of myosin VI toward the nucleus, rather than its nuclear import. However, the prominent and punctate localization of muskelin itself, as detected in the majority of neuronal nuclei, suggests that it potentially stays associated with myosin VI and perhaps supports the process of nuclear import. Furthermore, we found muskelin and myosin VI puncta to frequently colocalize in neuronal nuclei, and myosin VI was reported to accumulate in discrete puncta in the nucleus associated with RNAPII, PML nuclear bodies and nuclear speckles. Given the role of myosin VI in cellular processes such as proliferation, survival, cell adhesion, and migration (Cho and Chen, 2010; Fili et al., 2017; Hari-Gupta et al., 2020; Jung

et al., 2006; Loikkanen et al., 2009; Vreugde et al., 2006; Zorca et al., 2015), it is noteworthy that muskelin and other CTLH complex-associated proteins that contain the LisH/CTLH motifs were reported to essentially affect the same fundamental processes as discussed for myosin VI (Huffman et al., 2019; Lampert et al., 2018; Liu and Pfirrmann, 2019; Maitland et al., 2019; Qiao et al., 2020). Consistent with these cellular functions both, myosin VI and muskelin are reported to show significant association with breast and prostate cancers (Chen et al., 2019; Dunn et al., 2006; Gueron et al., 2014; Jung et al., 2019; Wang et al., 2015; Yoshida et al., 2004). Intriguingly, an affinity-based approach to screen for binding partners of the *Drosophila* homolog of myosin VI (Jaguar) identified muskelin and the other six CTLH complex members to associate with myosin VI (Finan et al., 2011). Therefore, the possible nuclear functions of muskelin and other CTLH complex members, as well as the question to what extent these functions may overlap with myosin VI-regulated nuclear processes, warrants further investigation.

In summary, our data identify that myosin VI nuclear localization is regulated through the dynein motor complex and muskelin. They suggest a mechanism by which MT-dependent dynein piggybacks the myosin motor to reach the neuronal nucleus. To our knowledge, this is one of the first reports providing evidence that myosin motors can actively be positioned to reach specific subcellular compartments by means of MT-based cytoskeleton transport.

Limitations of the study

In this study, we analyzed cultured primary hippocampal neurons and whole brain fractions of genetically modified mice for myosin VI nuclear targeting. In the future, it will be interesting to see whether dynein and muskelin regulate myosin VI nuclear delivery also in other cell types of the brain. The dynein-muskelin-assisted trafficking pathway might further be important in tissues where myosin VI nuclear functions were initially described, including cervical-, breast-, and adrenal gland cell lines. Although myosin VI was suggested to regulate hormone- and cytokine receptor-dependent nuclear functions in these tissues, future studies are warranted to investigate whether these triggers also affect myosin VI nuclear translocation and function in neurons.

In addition, we like to mention the technical limitations of the study. As the dynein transport machinery is important for a variety of cellular processes, the tools to only interfere with one isolated dynein-mediated process are limited. With respect to our study, overexpression of dynamitin in transgenic mice or transiently in cultured cells has previously been shown not only to inhibit MT-based dynein-mediated transport but also to affect Golgi morphology (Burkhardt et al., 1997; LaMonte et al., 2002; Valetti et al., 1999). A subpopulation of myosin VI reported to associate with the Golgi (Tumbarello et al., 2013) might therefore also undergo redistribution following dynamitin overexpression. Although we additionally applied the first dynein-specific chemical antagonist ciliobrevin in acute treatments (80 min, 20 μM), a dose-dependent effect of ciliobrevins (4-h treatment) on Golgi morphology has previously been observed (See et al., 2016). Importantly, depletion of the direct dynein adaptor muskelin, which does not localize to the Golgi, but regulates long-distance transport of synaptic cargo (Heisler et al., 2011, 2018), revealed comparable and similarly pronounced effects on myosin VI nuclear targeting when compared with dynein inhibition.

Resource availability

Lead contact

Further information and request for resources should be directed to and will be fulfilled by the lead contact, Frank F. Heisler (frank.heisler@zmnh.uni-hamburg.de).

Materials availability

All unique/stable reagents generated in this study are available from the lead contact with a completed Materials Transfer Agreement.

Data and code availability

All data are included in the manuscript.

METHODS

All methods can be found in the accompanying transparent methods supplemental file.

SUPPLEMENTAL INFORMATION

Supplemental information can be found online at https://doi.org/10.1016/j.isci.2021.102416.

ACKNOWLEDGMENTS

We are grateful to Erika L. F. Holzbaur for tissue lysates of transgenic mice overexpressing dynamitin. We also thank Michaela Schweizer for expertise in electron microscopy and Yvonne Pechmann for technical support. This work was supported by the Deutsche Forschungsgemeinschaft grant KN556/16-1 to M.K. and by the Deutsche Forschungsgemeinschaft FOR 2419 grants, project KN556/11-2 to M.K. and project HE8413/1-1 to F.F.H., Landesforschungsförderung Hamburg LFF-FV74 and LFF-FV76 to M.K., and the Ritz-Stiftung to F.F.H.

AUTHOR CONTRIBUTION

F.F.H. and M.K. designed and coordinated the project. F.F.H., N.S.-R., and M.M. performed the experiments. F.F.H. and M.K. analyzed the data. F.F.H. and M.K. wrote the manuscript and prepared the figures.

DECLARATION OF INTEREST

The authors declare no competing interests.

Received: July 9, 2020
Revised: February 15, 2021
Accepted: April 7, 2021
Published: May 21, 2021

REFERENCES

Adams, J.C., Seed, B., and Lawler, J. (1998). Muskelin, a novel intracellular mediator of cell adhesive and cytoskeletal responses to thrombospondin-1. EMBO J. *17*, 4964–4974.

Altman, D., Sweeney, H.L., and Spudich, J.A. (2004). The mechanism of myosin VI translocation and its load-induced anchoring. Cell *116*, 737–749.

Avraham, K.B., Hasson, T., Steel, K.P., Kingsley, D.M., Russell, L.B., Mooseker, M.S., Copeland, N.G., and Jenkins, N.A. (1995). The mouse Snell's waltzer deafness gene encodes an unconventional myosin required for structural integrity of inner ear hair cells. Nat. Genet. *11*, 369–375.

Boecker, C.A., and Holzbaur, E.L. (2019). Vesicular degradation pathways in neurons: at the crossroads of autophagy and endo-lysosomal degradation. Curr. Opin. Neurobiol. *57*, 94–101.

Burkhardt, J.K., Echeverri, C.J., Nilsson, T., and Vallee, R.B. (1997). Overexpression of the dynamitin (p50) subunit of the dynactin complex disrupts dynein-dependent maintenance of membrane organelle distribution. J. Cell Biol *139*, 469–484.

Buss, F., Arden, S.D., Lindsay, M., Luzio, J.P., and Kendrick-Jones, J. (2001). Myosin VI isoform localized to clathrin-coated vesicles with a role in clathrin-mediated endocytosis. EMBO J. *20*, 3676–3684.

Chen, B., Zhang, C., Wang, Z., Chen, Y., Xie, H., Li, S., Liu, X., Liu, Z., and Chen, P. (2019). Mechanistic insights into Nav1.7-dependent regulation of rat prostate cancer cell invasiveness revealed by toxin probes and proteomic analysis. FEBS J. *286*, 2549–2561.

Cho, S.J., and Chen, X. (2010). Myosin VI is differentially regulated by DNA damage in p53- and cell type-dependent manners. J. Biol. Chem. *285*, 27159–27166.

Coles, C.H., and Bradke, F. (2015). Coordinating neuronal actin-microtubule dynamics. Curr. Biol. *25*, R677–R691.

Cook, A.W., Gough, R.E., and Toseland, C.P. (2020). Nuclear myosins - roles for molecular transporters and anchors. J. Cell Sci. *133*, jcs242420.

Delto, C.F., Heisler, F.F., Kuper, J., Sander, B., Kneussel, M., and Schindelin, H. (2015). The LisH motif of muskelin is crucial for oligomerization and governs intracellular localization. Structure *23*, 364–373.

Dunn, T.A., Chen, S., Faith, D.A., Hicks, J.L., Platz, E.A., Chen, Y., Ewing, C.M., Sauvageot, J., Isaacs, W.B., De Marzo, A.M., and Luo, J. (2006). A novel role of myosin VI in human prostate cancer. Am. J. Pathol. *169*, 1843–1854.

Emes, R.D., and Ponting, C.P. (2001). A new sequence motif linking lissencephaly, Treacher Collins and oral-facial-digital type 1 syndromes, microtubule dynamics and cell migration. Hum. Mol. Genet. *10*, 2813–2820.

Falk, M., Lukasova, E., and Kozubek, S. (2008). Chromatin structure influences the sensitivity of DNA to gamma-radiation. Biochim. Biophys. Acta *1783*, 2398–2414.

Fili, N., Hari-Gupta, Y., Aston, B., Dos Santos, A., Gough, R.E., Alamad, B., Wang, L., Martin-Fernandez, M.L., and Toseland, C.P. (2020). Competition between two high- and low-affinity protein-binding sites in myosin VI controls its cellular function. J. Biol. Chem. *295*, 337–347.

Fili, N., Hari-Gupta, Y., Dos Santos, A., Cook, A., Poland, S., Ameer-Beg, S.M., Parsons, M., and Toseland, C.P. (2017). NDP52 activates nuclear myosin VI to enhance RNA polymerase II transcription. Nat. Commun. *8*, 1871.

Finan, D., Hartman, M.A., and Spudich, J.A. (2011). Proteomics approach to study the functions of Drosophila myosin VI through identification of multiple cargo-binding proteins. Proc. Natl. Acad. Sci. U S A *108*, 5566–5571.

Firestone, A.J., Weinger, J.S., Maldonado, M., Barlan, K., Langston, L.D., O'Donnell, M., Gelfand, V.I., Kapoor, T.M., and Chen, J.K. (2012). Small-molecule inhibitors of the AAA+ ATPase motor cytoplasmic dynein. Nature *484*, 125–129.

Franchini, L., Stanic, J., Ponzoni, L., Mellone, M., Carrano, N., Musardo, S., Zianni, E., Olivero, G., Marcello, E., Pittaluga, A., et al. (2019). Linking NMDA receptor synaptic retention to synaptic plasticity and cognition. iScience *19*, 927–939.

Gauthier, L.R., Charrin, B.C., Borrell-Pages, M., Dompierre, J.P., Rangone, H., Cordelieres, F.P., De Mey, J., MacDonald, M.E., Lessmann, V., Humbert, S., and Saudou, F. (2004). Huntingtin controls neurotrophic support and survival of neurons by enhancing BDNF vesicular transport along microtubules. Cell *118*, 127–138.

Grosse-Berkenbusch, A., Hettich, J., Kuhn, T., Fili, N., Cook, A., Hari-Gupta, Y., Palmer, A., Streit, L., Ellis, P.J.I., Toseland, C.P., and Gebhardt, J.C.M. (2020). Myosin VI moves on nuclear actin filaments and supports long-range chromatin rearrangements. bioRxiv. https://doi.org/10.1101/2020.04.03.023614.

Gueron, G., Giudice, J., Valacco, P., Paez, A., Elguero, B., Toscani, M., Jaworski, F., Leskow, F.C., Cotignola, J., Marti, M., et al. (2014). Heme-oxygenase-1 implications in cell morphology and the adhesive behavior of prostate cancer cells. Oncotarget *5*, 4087–4102.

Hanz, S., Perlson, E., Willis, D., Zheng, J.Q., Massarwa, R., Huerta, J.J., Koltzenburg, M., Kohler, M., van-Minnen, J., Twiss, J.L., and Fainzilber, M. (2003). Axoplasmic importins enable retrograde injury signaling in lesioned nerve. Neuron *40*, 1095–1104.

Hari-Gupta, Y., Fili, N., Dos Santos, A., Cook, A., Gough, R.E., Reed, H.C.W., Wang, L., Aaron, J., Venit, T., Wait, E., et al. (2020). Nuclear myosin VI regulates the spatial organization of mammalian transcription initiation. bioRxiv. https://doi.org/10.1101/2020.04.21.053124.

Heerssen, H.M., Pazyra, M.F., and Segal, R.A. (2004). Dynein motors transport activated Trks to promote survival of target-dependent neurons. Nat. Neurosci. *7*, 596–604.

Heisler, F.F., Lee, H.K., Gromova, K.V., Pechmann, Y., Schurek, B., Ruschkies, L., Schroeder, M., Schweizer, M., and Kneussel, M. (2014). GRIP1 interlinks N-cadherin and AMPA receptors at vesicles to promote combined cargo transport into dendrites. Proc. Natl. Acad. Sci. U S A *111*, 5030–5035.

Heisler, F.F., Loebrich, S., Pechmann, Y., Maier, N., Zivkovic, A.R., Tokito, M., Hausrat, T.J., Schweizer, M., Bahring, R., Holzbaur, E.L., et al. (2011). Muskelin regulates actin filament- and microtubule-based GABA(A) receptor transport in neurons. Neuron *70*, 66–81.

Heisler, F.F., Pechmann, Y., Wieser, I., Altmeppen, H.C., Veenendaal, L., Muhia, M., Schweizer, M., Glatzel, M., Krasemann, S., and Kneussel, M. (2018). Muskelin coordinates PrP(C) lysosome versus exosome targeting and impacts prion disease progression. Neuron *99*, 1155–1169 e1159.

Herbst, W.A., and Martin, K.C. (2017). Regulated transport of signaling proteins from synapse to nucleus. Curr. Opin. Neurobiol. *45*, 78–84.

Hirokawa, N., Niwa, S., and Tanaka, Y. (2010). Molecular motors in neurons: transport mechanisms and roles in brain function, development, and disease. Neuron *68*, 610–638.

Huffman, N., Palmieri, D., and Coppola, V. (2019). The CTLH complex in cancer cell plasticity. J. Oncol. *2019*, 4216750.

Jung, E.J., Liu, G., Zhou, W., and Chen, X. (2006). Myosin VI is a mediator of the p53-dependent cell survival pathway. Mol. Cell. Biol. *26*, 2175–2186.

Jung, S.Y., Papp, J.C., Sobel, E.M., Yu, H., and Zhang, Z.F. (2019). Breast cancer risk and insulin resistance: post genome-wide gene-environment interaction study using a random survival forest. Cancer Res. *79*, 2784–2794.

Karolczak, J., Sobczak, M., Majewski, L., Yeghiazaryan, M., Jakubiec-Puka, A., Ehler, E., Slawinska, U., Wilczynski, G.M., and Redowicz, M.J. (2013). Myosin VI in skeletal muscle: its localization in the sarcoplasmic reticulum, neuromuscular junction and muscle nuclei. Histochem. Cell Biol. *139*, 873–885.

Karpova, A., Mikhaylova, M., Bera, S., Bar, J., Reddy, P.P., Behnisch, T., Rankovic, V., Spilker, C., Bethge, P., Sahin, J., et al. (2013). Encoding and transducing the synaptic or extrasynaptic origin of NMDA receptor signals to the nucleus. Cell *152*, 1119–1133.

King, S.J., and Schroer, T.A. (2000). Dynactin increases the processivity of the cytoplasmic dynein motor. Nat. Cell Biol. *2*, 20–24.

Kneussel, M., Triller, A., and Choquet, D. (2014). SnapShot: receptor dynamics at plastic synapses. Cell *157*, 1738–1738 e1731.

Kneussel, M., and Wagner, W. (2013). Myosin motors at neuronal synapses: drivers of membrane transport and actin dynamics. Nat. Rev. Neurosci. *14*, 233–247.

LaMonte, B.H., Wallace, K.E., Holloway, B.A., Shelly, S.S., Ascano, J., Tokito, M., Van Winkle, T., Howland, D.S., and Holzbaur, E.L. (2002). Disruption of dynein/dynactin inhibits axonal transport in motor neurons causing late-onset progressive degeneration. Neuron *34*, 715–727.

Lampert, F., Stafa, D., Goga, A., Soste, M.V., Gilberto, S., Olieric, N., Picotti, P., Stoffel, M., and Peter, M. (2018). The multi-subunit GID/CTLH E3 ubiquitin ligase promotes cell proliferation and targets the transcription factor Hbp1 for degradation. Elife *7*, e35528.

Lever, M.B., Karpova, A., and Kreutz, M.R. (2015). An Importin Code in neuronal transport from synapse-to-nucleus? Front. Mol. Neurosci. *8*, 33.

Liu, H., and Pfirrmann, T. (2019). The Gid-complex: an emerging player in the ubiquitin ligase league. Biol. Chem. *400*, 1429–1441.

Loikkanen, I., Toljamo, K., Hirvikoski, P., Vaisanen, T., Paavonen, T.K., and Vaarala, M.H. (2009). Myosin VI is a modulator of androgen-dependent gene expression. Oncol. Rep. *22*, 991–995.

Maas, C., Tagnaouti, N., Loebrich, S., Behrend, B., Lappe-Siefke, C., and Kneussel, M. (2006). Neuronal cotransport of glycine receptor and the scaffold protein gephyrin. J. Cell Biol. *172*, 441–451.

Maitland, M.E.R., Onea, G., Chiasson, C.A., Wang, X., Ma, J., Moor, S.E., Barber, K.R., Lajoie, G.A., Shaw, G.S., and Schild-Poulter, C. (2019). The mammalian CTLH complex is an E3 ubiquitin ligase that targets its subunit muskelin for degradation. Sci. Rep. *9*, 9864.

Majewski, L., Nowak, J., Sobczak, M., Karatsai, O., Havrylov, S., Lenartowski, R., Suszek, M., Lenartowska, M., and Redowicz, M.J. (2018). Myosin VI in the nucleus of neurosecretory PC12 cells: stimulation-dependent nuclear translocation and interaction with nuclear proteins. Nucleus *9*, 125–141.

Morris, S.M., Arden, S.D., Roberts, R.C., Kendrick-Jones, J., Cooper, J.A., Luzio, J.P., and Buss, F. (2002). Myosin VI binds to and localises with Dab2, potentially linking receptor-mediated endocytosis and the actin cytoskeleton. Traffic *3*, 331–341.

Mullen, R.J., Buck, C.R., and Smith, A.M. (1992). NeuN, a neuronal specific nuclear protein in vertebrates. Development *116*, 201–211.

Olenick, M.A., Dominguez, R., and Holzbaur, E.L.F. (2019). Dynein activator Hook1 is required for trafficking of BDNF-signaling endosomes in neurons. J. Cell Biol. *218*, 220–233.

Olenick, M.A., and Holzbaur, E.L.F. (2019). Dynein activators and adaptors at a glance. J. Cell Sci. *132*, jcs227132.

Osterweil, E., Wells, D.G., and Mooseker, M.S. (2005). A role for myosin VI in postsynaptic structure and glutamate receptor endocytosis. J. Cell Biol. *168*, 329–338.

Otmakhov, N., Khibnik, L., Otmakhova, N., Carpenter, S., Riahi, S., Asrican, B., and Lisman, J. (2004). Forskolin-induced LTP in the CA1 hippocampal region is NMDA receptor dependent. J. Neurophysiol. *91*, 1955–1962.

Palazzo, A.F., Joseph, H.L., Chen, Y.J., Dujardin, D.L., Alberts, A.S., Pfister, K.K., Vallee, R.B., and Gundersen, G.G. (2001). Cdc42, dynein, and dynactin regulate MTOC reorientation independent of Rho-regulated microtubule stabilization. Curr. Biol. *11*, 1536–1541.

Perlson, E., Hanz, S., Ben-Yaakov, K., Segal-Ruder, Y., Seger, R., and Fainzilber, M. (2005). Vimentin-dependent spatial translocation of an activated MAP kinase in injured nerve. Neuron *45*, 715–726.

Perlson, E., Jeong, G.B., Ross, J.L., Dixit, R., Wallace, K.E., Kalb, R.G., and Holzbaur, E.L. (2009). A switch in retrograde signaling from survival to stress in rapid-onset neurodegeneration. J. Neurosci. *29*, 9903–9917.

Qiao, S., Langlois, C.R., Chrustowicz, J., Sherpa, D., Karayel, O., Hansen, F.M., Beier, V., von Gronau, S., Bollschweiler, D., Schafer, T., et al. (2020). Interconversion between anticipatory and active GID E3 ubiquitin ligase conformations via metabolically driven substrate receptor assembly. Mol. Cell *77*, 150–163 e159.

Reck-Peterson, S.L., Redwine, W.B., Vale, R.D., and Carter, A.P. (2018). The cytoplasmic dynein transport machinery and its many cargoes. Nat. Rev. Mol. Cell Biol. *19*, 382–398.

Sahlender, D.A., Roberts, R.C., Arden, S.D., Spudich, G., Taylor, M.J., Luzio, J.P., Kendrick-Jones, J., and Buss, F. (2005). Optineurin links myosin VI to the Golgi complex and is involved in Golgi organization and exocytosis. J. Cell Biol. *169*, 285–295.

Schapitz, I.U., Behrend, B., Pechmann, Y., Lappe-Siefke, C., Kneussel, S.J., Wallace, K.E., Stempel, A.V., Buck, F., Grant, S.G., Schweizer, M., et al. (2010). Neuroligin 1 is dynamically exchanged at postsynaptic sites. J. Neurosci. *30*, 12733–12744.

Schliwa, M., and Woehlke, G. (2003). Molecular motors. Nature *422*, 759–765.

See, S.K., Hoogendoorn, S., Chung, A.H., Ye, F., Steinman, J.B., Sakata-Kato, T., Miller, R.M., Cupido, T., Zalyte, R., Carter, A.P., et al. (2016). Cytoplasmic dynein antagonists with improved potency and isoform selectivity. ACS Chem. Biol. *11*, 53–60.

Tumbarello, D.A., Kendrick-Jones, J., and Buss, F. (2013). Myosin VI and its cargo adaptors - linking endocytosis and autophagy. J. Cell Sci. *126*, 2561–2570.

Vale, R.D. (2003). The molecular motor toolbox for intracellular transport. Cell *112*, 467–480.

Valetti, C., Wetzel, D.M., Schrader, M., Hasbani, M.J., Gill, S.R., Kreis, T.E., and Schroer, T.A. (1999). Role of dynactin in endocytic traffic: effects of dynamitin overexpression and colocalization with CLIP-170. Mol. Biol. Cell *10*, 4107–4120.

Valiyaveettil, M., Bentley, A.A., Gursahaney, P., Hussien, R., Chakravarti, R., Kureishy, N., Prag, S., and Adams, J.C. (2008). Novel role of the muskelin-RanBP9 complex as a nucleocytoplasmic mediator of cell morphology regulation. J. Cell Biol. *182*, 727–739.

Vreugde, S., Ferrai, C., Miluzio, A., Hauben, E., Marchisio, P.C., Crippa, M.P., Bussi, M., and Biffo, S. (2006). Nuclear myosin VI enhances RNA polymerase II-dependent transcription. Mol. Cell *23*, 749–755.

Wagner, W., Lippmann, K., Heisler, F.F., Gromova, K.V., Lombino, F.L., Roesler, M.K., Pechmann, Y., Hornig, S., Schweizer, M., Polo, S., et al. (2019). Myosin VI drives clathrin-mediated AMPA receptor endocytosis to facilitate cerebellar long-term depression. Cell Rep. *28*, 11–20 e19.

Wang, H., Wang, B., Zhu, W., and Yang, Z. (2015). Lentivirus-mediated knockdown of myosin VI inhibits cell proliferation of breast cancer cell. Cancer Biother. Radiopharm. *30*, 330–335.

Wells, A.L., Lin, A.W., Chen, L.Q., Safer, D., Cain, S.M., Hasson, T., Carragher, B.O., Milligan, R.A., and Sweeney, H.L. (1999). Myosin VI is an actin-based motor that moves backwards. Nature *401*, 505–508.

Yoshida, H., Cheng, W., Hung, J., Montell, D., Geisbrecht, E., Rosen, D., Liu, J., and Naora, H. (2004). Lessons from border cell migration in the Drosophila ovary: a role for myosin VI in dissemination of human ovarian cancer. Proc. Natl. Acad. Sci. U S A *101*, 8144–8149.

Zorca, C.E., Kim, L.K., Kim, Y.J., Krause, M.R., Zenklusen, D., Spilianakis, C.G., and Flavell, R.A. (2015). Myosin VI regulates gene pairing and transcriptional pause release in T cells. Proc. Natl. Acad. Sci. U S A *112*, E1587–E1593.

iScience, Volume *24*

Supplemental information

Dynein and muskelin control myosin VI delivery towards the neuronal nucleus

Matthias Kneussel, Noelia Sánchez-Rodríguez, Michaela Mischak, and Frank F. Heisler

Transparent Methods

Mouse lines

All experiments were in accordance with the recommendations in the Guide for the Care and Use of Laboratory Animals of the German Animal Welfare Act on protection of animals. The protocol was approved by the Ethical Committee of the Freie und Hansestadt Hamburg, Amt für Gesundheit und Verbraucherschutz (Permit number: V 1300/591-00.33). Generation of muskelin knockout mice was previously described (Heisler et al., 2011). B6;129/SvEv-Mkln1$^{Gt(OST448976)Lex}$/J mice were backcrossed to C57BL/6J. Snell's waltzer mice, in which homozygous mutant mice (sv/sv) contain two null mutation alleles to functionally deplete myosin VI, were obtained from The Jackson Laboratory (B6 x STOCK Tyrc-ch Bmp5se +/+ Myo6sv/J) and were on a C57BL/6J background. Samples of transgenic mice overexpressing dynamitin in brain (Tg(Thy1-DCTN2)M21Elfh) were obtained from Erika Holzbaur (Pennsylvania, PA) (LaMonte et al., 2002; Perlson et al., 2009). All mice were maintained in a pathogen-free, temperature- and humidity-controlled vivarium on a 12 h light/dark schedule. Mice had access to standard laboratory chow and water ad libitum. Both male and female mice were included in all of the experiments. In general, littermates of the appropriate genotypes were used.

Primary neuronal culture

Primary mouse hippocampal neurons were prepared from P0 newborn mice, as previously described (Heisler et al., 2014), plated at 90,000 to 110,000 cells/well onto poly-L-lysine- (Sigma, Steinheim, Germany) coated 24 well plates (Greiner Bio-One, Kremsmünster, Austria). Cells were cultured in PNGM Primary Neuron Basal Medium supplemented with PNGM-A Single Quots (PA, OA, NSF-1, L-Glutamine) (all Lonza Group Ltd., Basel, Switzerland) and 100U/mL penicillin and 100**m**g/mL streptomycin (all Invitrogen, Carlsbad, CA) at 37°C in a humidified incubator with 5%

CO2. Cells cultured between 10 and 11 days in vitro (DIV 10-11) were used for transfection with a calcium phosphate coprecipitation method (Heisler et al., 2014) or with Lipofectamine 2000 (Invitrogen, Carlsbad, CA). Cultured neurons were subjected to immunostaining at DIV 12-14.

Antibodies

The following antibodies were used for immunoprecipitation (IP) and western blotting (WB): mouse anti-Dynein Intermediate Chain (5 µg (IP) and 1:3,000 (WB), Chemicon, Hofheim, Germany); rabbit anti-Myosin VI (4 µg (IP) and 1:2,000 (WB), Sigma, Taufkirchen, Germany); rabbit anti-Myosin VI (1:200 (WB) Santa Cruz Biotechnology, Heidelberg, Germany); guinea pig anti-Muskelin (5 µg (IP) and 1:3,000 (WB), (Tagnaouti et al., 2007); rabbit anti-GluN2B (1:500 (WB), Abcam, Cambridge, UK); mouse anti NeuN (1:500 (WB), Millipore, Temecula, CA); rabbit anti-Actin (1:2,000 (WB), Sigma, Taufkirchen, Germany); mouse unspecific IgG (5 µg (IP), Sigma, Taufkirchen, Germany); guinea pig unspecific IgG (5 µg (IP), Santa Cruz Biotechnology, Heidelberg, Germany); peroxidase-conjugated goat anti-guinea pig, goat anti-rabbit and goat anti-mouse (all 1:15,000, Dianova, Hamburg, Germany). The following antibodies were used for immunofluorescence: guinea pig anti-Muskelin (1:50, (Tagnaouti et al., 2007)); goat anti-Myosin VI (1:50, Santa Cruz Biotechnology, Heidelberg, Germany); rabbit anti-Myosin VI (1:100, Sigma, Taufkirchen, Germany); CY3- or CY5-conjugated donkey anti-guinea pig or donkey anti-goat (all 1:500, Dianova, Hamburg, Germany); Alexa Fluor 488 conjugated donkey anti-guinea pig or donkey anti-goat (40µg/ml, Invitrogen, Carlsbad, CA).

Constructs

EGFP-Dynamitin has been previously described (Palazzo et al., 2001). To generate EGFP-MyoVIdn, the entire *myo VI* tail domain was amplified from rat cDNA by PCR, a-tailed and ligated into pGEM-Teasy. It was cloned as *SalI-EcoRI* fragment into

pEGFP-C2 (BD Biosciences, Heidelberg, Germany). All constructs were verified by dideoxy sequencing.

Cellular fractionation and isolation of nuclear proteins

Nuclear and cytoplasmic fractions were obtained from fresh mouse brain tissue by using a Nuclear Extract Kit (Active Motive, Carlsbad, CA). Briefly, whole brains of adult mice were sliced into 1 mm sections in ice-cold Hypotonic Buffer containing phosphatase and protease inhibitors supplemented with DTT and Detergent (Active Motive, Carlsbad, CA). A dounce homogenizer with large-clearance Teflon pestle (Sartorius Group, Goettingen, Germany) was used for homogenization until the cells were dissociated. Cells were collected by centrifugation at 850 x g for 10 min and subjected to cytoplasmic and nuclear fractionation following the manufacturers protocol (Active Motive, Carlsbad, CA).

Coimmunoprecipitation

For coimmunoprecipitation experiments, whole brains of adult mice were dissected in ice cold PBS and homogenized in IM-Ac buffer (20mM HEPES, 100mM KAc, 40mM KCl, 5mM EGTA, 5mM $MgCl_2$, pH 7.2) with freshly added proteinase inhibitor cocktail (Roche, Mannheim, Germany), 1mM PMSF, 5mM DTT and 2mM Mg-ATP (all Sigma, Taufkirchen, Germany). The homogenate was clarified by centrifugation at 1,000 x g for 10 min and the postnuclear supernatant (S1) used for the following steps. After coupling 5 µg of antibodies to magnetic Protein G Dynabeads for 4 to 5h (Invitrogen, Carlsbad, CA), 1% Triton-X-100 preincubated extracts from S1 were incubated with antibody-coupled beads overnight, followed by extensive washing steps (4-6) with IP-buffer (150mM NaCl, 50mM Tris, pH 7.5, 5mM $MgCl_2$) containing 1% Triton X-100. Bound proteins were eluted in SDS sample buffer, subjected to SDS-PAGE and analyzed by Western blotting.

Ciliobrevin D and cLTP experiments

DIV 12-14 dissociated mouse hippocampal neurons were treated with 20 µM Ciliobrevin D (Merck, Darmstadt, Germany) or 0.4% DMSO (control) (Sigma, Taufkirchen, Germany) for 80 min at 37°C in a humidified incubator with 5% CO2. For experiments involving cLTP inductions, neurons were pretreated with 20 µM Ciliobrevin D or with 0.4% DMSO (control) for 40 min. cLTP was induced by treatment with 50 µM Forskolin, 100 nM Rolipram and 100 µM Picrotoxin (Franchini et al., 2019; Otmakhov et al., 2004) (all Tocris, Wiesbaden-Nordenstadt, Germany) for 10 min in Ringer solution without Mg^{2+} (125 mM NaCl, 2,5 mM KCl, 3 mM $CaCl^2$, 33 mM D-Glucose, 25 mM HEPES, pH 7.3) (all Sigma) and in the presence of either 0.4% DMSO or 20 µM Ciliobrevin D. Neurons were then washed once with warm PBS and for cLTP recovery incubated for 30 min in Ringer solution containing Mg^{2+} (125 mM NaCl, 2,5 mM KCl, 2 mM $CaCl^2$, 33 mM D-Glucose, 1 mM $MgCl^2$, 25 mM HEPES, pH 7.3), in the presence of either 0.4% DMSO or 20 µM Ciliobrevin D. Neurons were further processed as described in immunocytochemistry section.

Immunocytochemistry

DIV 12-14 primary cultured mouse hippocampal neurons from wildtype, muskelin knockout mice or after transfection, were fixed in 4% PFA/4% sucrose (10 min) and washed in PBS prior to permeabilization with 0.25% Triton X-100 (5 min). Unspecific binding sites were blocked with 3% (w/v) bovine serum albumin (Applichem, Darmstadt, Germany) for 1 h and cells were incubated with primary antibodies overnight at 4°C. Cells were washed three times in PBS and incubated with secondary antibodies for 1 h and with TO-PRO-3 or DAPI (both 1:1,000, Thermo Scientific, Waltham, MA) if applicable, washed extensively and mounted in Aqua Poly Mount (Polysciences, Warrington, PA). For microscopy analysis an upright Laser-scanning Confocal Microscope Fluoview FV1000 with Olympus Fluoview Software Ver. 2.1.b (Olympus, Hamburg, Germany) or an inverted Leica TCS-SP2 laser

scanning confocal microscope (Leica Microsystems, Wetzlar, Germany) was used. For double-labeling studies, a sequential scanning mode was applied.

Electron microscopy

Mice were anaesthetized and perfused with 4% PFA and 0.1% glutaraldehyde in 0.1 M phosphate buffer (PB, pH 7.4) for preembedding immunohistochemistry. Sagittal vibratome sections of the hippocampus were cut into 150 nm and immersed in 2.3 mol/L sucrose in PB, overnight, at 4°C for cryoprotection. Thereafter they were subjected to two freeze-thaw cycles in liquid nitrogen to aid penetration of immunoreagents and first treated with 1% $NaBH_4$ and then with 0.3% H_2O_2 in PBS for 30 min. After rinsing in PBS, sections were blocked with 10% horse serum (HS) containing 0.2% bovine serum albumin (BSA) for 15 min and left overnight with primary antibody (guinea pig anti Muskelin (Tagnaouti et al., 2007), 1:100) in carrier containing PBS with 1% PS and 0.2% BSA. Sections were washed in PBS, incubated with biotinylated secondary antibody (Vector Labs, Burlingame, CA) diluted in carrier for 90 min. After rinsing, sections were incubated with ABC (Vector Labs), diluted to a 1:100 concentration in PBS for 90 min. Afterwards they were washed in PBS and further incubated in diaminobenzidine (DAB)-H_20_2 solution (Sigma, Taufkirchen, Germany) for 10 min. The 150 µm thick sections were postfixed with 1% OsO_4, dehydrated in an ascending series of ethanol and embedded in Epon (Carl Roth GmbH & Co. KG, Karlsruhe, Germany). Ultrathin sections were then examined with a Zeiss EM 902 (Zeiss, Göttingen, Germany).

General Statistical Analysis

The sample size was adjusted according to results of prior pilot datasets or studies that used similar methods or paradigms. Data were analyzed using Microsoft Excel, GraphPad Prism6.07 (GraphPad Software, La Jolla, CA) and IBM SPSS Statistics 22 (IBM, Armonk, NY). Prior to analysis, data were explored by using IBM SPSS

Statistics 22. Data were explored for normality within sample groups by using the Shapiro-Wilk test and for equality of variances between sample groups by using the Levene´s test. For non-parametric data, we used the Kruskal-Wallis ANOVA and the Mann-Whitney U test. Dunn´s pairwise multiple comparisons with p values adjusted using the Bonferroni correction were calculated when applicable. A two-sample Kolmogorov-Smirnov test was used to compare the distribution between sample groups. For parametric data, the independent samples t test was used. All statistical tests used, as well as the corresponding p and n values are specified in the accompanying figure legends for each experiment. In general, an error rate of $p < 0.05$ was adopted as a yardstick for statistical significance; *: $p < 0.05$ significant, **: $p < 0.01$ very significant, ***: $p < 0.001$ highly significant. All experiments were repeated at least three times using independent primary neuron cultures or mice from individual animal litters. Parametric data are reported as mean ± the classical 95% confidence intervals for the mean. Parametric data are visualized in column scatter plots showing individual data points, and with error bars representing the 95% confidence intervals for the mean. Non-parametric data are reported as median and visualized in box and whisker plots (Tukey style). Box borders indicate the 25th and 75th percentiles, horizontal lines inside boxes indicate the median, and whiskers represent values less than 1.5 times the interquartile range lower or higher than the 25th and 75th percentiles, respectively. We added red squares to indicate the mean.

Western Blot and Confocal Image Data Analysis

For evaluation of relative immunoblot signal intensities, images were acquired using a Chemo-Cam Imager ECL HR 16-3200 (Intas, Goettingen, Germany) or GE Healthcare Amersham Hyperfilm ECL (Thermo Scientific, Waltham, MA). Immunoblot signal intensities were analyzed using the ImageJ, version 1.38, software (National Institutes of Health, NIH). Intensities were then normalized, as compared to loading control signals or to self-precipitation in case of coimmunoprecipitation experiments.

Fluorescence imaging was carried out with an upright Laser-scanning Confocal Microscope Fluoview FV1000 with Olympus Fluoview Software Ver. 2.1.b (Olympus, Hamburg, Germany) or an inverted Leica TCS-SP2 laser scanning confocal microscope (Leica Microsystems, Wetzlar, Germany) using a 63x objective. For simultaneous multiple-channel fluorescence, images were taken in a sequential channel recording mode. Confocal images from multiple individual cells used for statistical analysis were obtained using identical photomultiplier values throughout each experiment. All experiments were at least replicated three times using different culture preparations or animal litters. Images were saved as overlay TIF-files and further processed offline and analyzed using MetaMorph 7.1 (Molecular Devices, San Jose, CA). First regions of interests (ROIs) were defined using the ROI tool. Overlay TIF-files were separated in green, red or blue channels using the “color separate” function. ROIs were transferred from overlay to each channel using the “transfer region” function. For definition of image thresholds, brightness was adjusted using the “Inclusive thresholding state” function. Fluorescence intensity and area measurements were performed using the “Integrated Morphometry Analysis” function. Intensity profiles along dendrites were created with the “line scan” function and correlation scatter plots as well as calculation of Pearson´s correlation coefficient was performed with MetaMorph “Correlation Plot” function. The percentage of area of colocalized signal A over B or vice versa, were calculated using the “Colocalization“ function of MetaMorph.

Supplemental References

Franchini, L., Stanic, J., Ponzoni, L., Mellone, M., Carrano, N., Musardo, S., Zianni, E., Olivero, G., Marcello, E., Pittaluga, A.*, et al.* (2019). Linking NMDA Receptor Synaptic Retention to Synaptic Plasticity and Cognition. iScience 19, 927-939.

Heisler, F.F., Lee, H.K., Gromova, K.V., Pechmann, Y., Schurek, B., Ruschkies, L., Schroeder, M., Schweizer, M., and Kneussel, M. (2014). GRIP1 interlinks N-cadherin and AMPA receptors at vesicles to promote combined cargo transport into dendrites. Proc Natl Acad Sci U S A 111, 5030-5035.

Heisler, F.F., Lee, H.K., Gromova, K.V., Pechmann, Y., Schurek, B., Ruschkies, L., Schroeder, M., Schweizer, M., and Kneussel, M. (2014). GRIP1 interlinks N-cadherin and AMPA receptors at vesicles to promote combined cargo transport into dendrites. Proc Natl Acad Sci U S A 111, 5030-5035.

LaMonte, B.H., Wallace, K.E., Holloway, B.A., Shelly, S.S., Ascano, J., Tokito, M., Van Winkle, T., Howland, D.S., and Holzbaur, E.L. (2002). Disruption of dynein/dynactin inhibits axonal transport in motor neurons causing late-onset progressive degeneration. Neuron 34, 715-727.

Otmakhov, N., Khibnik, L., Otmakhova, N., Carpenter, S., Riahi, S., Asrican, B., and Lisman, J. (2004). Forskolin-induced LTP in the CA1 hippocampal region is NMDA receptor dependent. J Neurophysiol 91, 1955-1962.

Palazzo, A.F., Joseph, H.L., Chen, Y.J., Dujardin, D.L., Alberts, A.S., Pfister, K.K., Vallee, R.B., and Gundersen, G.G. (2001). Cdc42, dynein, and dynactin regulate MTOC reorientation independent of Rho-regulated microtubule stabilization. Curr Biol 11, 1536-1541.

Perlson, E., Jeong, G.B., Ross, J.L., Dixit, R., Wallace, K.E., Kalb, R.G., and Holzbaur, E.L. (2009). A switch in retrograde signaling from survival to stress in rapid-onset neurodegeneration. J Neurosci 29, 9903-9917.

Tagnaouti, N., Loebrich, S., Heisler, F., Pechmann, Y., Fehr, S., De Arcangelis, A., Georges-Labouesse, E., Adams, J.C., and Kneussel, M. (2007). Neuronal expression of muskelin in the rodent central nervous system. BMC Neurosci 8, 28.